

Cyclic Fusion of Measuring Information in Curved Elastomer Contact via Vision-Based Tactile Sensing

Zilan Li, Zhibin Zou, Weiliang Xu, Yuanzhi Zhou, *Student Member, IEEE*, Guoyuan Zhou, Muxing Huang, Xuan Huang, and Xinning Li, *Member, IEEE*

Abstract—Using elastomer deformation to measure object surface features in tactile sensing is effective, as it captures microscale deformations through densely arranged optical imaging sensors that detect subtle data variations. To enable continuous contact recognition, elastomers are crafted with curved surfaces to adjust to changes in the contact area. However, this design leads to uneven deformations, distorting tactile images and inaccurately reflecting the true elastomer deformations. This inconsistency considerably reduces the utility of the tactile data. In this work, we propose a cyclic fusion strategy for vision-based tactile sensing for precise contact data extraction and shape feature integration at the pixel level. Utilizing frequency domain fusion, the system merges topography as indicated by elastomer deformation, enhancing information content by over 40% and preserving structural consistency. Further, this system could effectively extract and summarize micro-scale contact features, using neural networks to achieve a detection mAP of 90.90% and classification accuracy of 99.83%. Using this strategy, the measurement minimizes data interference, accurately depicting object morphology on tactile images and enhancing tactile sensation restoration.

Index Terms—Curved elastomers, cyclic fusion, feature measure, vision-based tactile sensing,

I. INTRODUCTION

Tactile sensing [1]-[4] is significant in various domains, including robotics [5], electronic skin [6], and human-computer interaction [7]. To obtain sufficiently trustworthy tactile information in more complex scenarios, vision-based tactile sensors [8][9] have garnered substantial attention in texture discrimination, surface analysis, and related research endeavors, owing to their exceptional integration and impressive resolution. In the sensing system, the inbuilt camera achieves tactile reproduction by capturing the deformation produced by the elastomer in the sensor during interaction with the object. In continuous sensing, for planar elastomers, if the position of the contact needs to be

This work was supported by the Guangdong Basic and Applied Basic Research Foundation (No. 2022A1515010136), the Guangdong Provincial Key Laboratory of Nanophotonic Functional Materials and Devices, and the South China Normal University start-up fund.

Zilan Li, Zhibin Zou, Weiliang Xu, Yuanzhi Zhou, Guoyuan Zhou, Muxing Huang, Xuan Huang, and Xinning Li are with the Guangdong Provincial Key Laboratory of Nanophotonic Functional Materials and Devices, Guangdong Basic Research Center of Excellence for Structure and Fundamental Interactions of Matter, School of Information and Optoelectronic Science and Engineering, South China Normal University, Guangzhou 510006, China (corresponding author e-mail: xmli@m.scnu.edu.cn).

changed, it is necessary to disengage from the object and then recontact it. This process leads to discontinuities in the acquisition. To overcome this difficulty, the elastomer can be arranged as a curved surface. The curved structure allows the elastomer to retain some areas out of contact and can be rolled to actively bring different locations in the structure into contact with the object, keeping the sensing system in contact at all times. This structural feature introduces the problem that the precise imaging plane of the camera does not match the curved surface of the contact structure. The accuracy of converting deformation data to images depends on the deformation occurring within the camera's effective focal length. However, in systems with curved contact structures, this condition isn't consistently met, disrupting the correlation between captured images and contact data. In addition, the measuring information cannot directly represent the actual morphology of the object due to the inconsistency of the contact morphology in the curved structures in each region.

Faced with this situation, the concern is to achieve a truthful recording and identification of the deformation variables of elastomers arranged on curved surfaces. An approach is to accurately align the system design and component arrangement to enable conversion from elastomer deformation to tactile images being accurately recognized. For example, the TacTip sensor has a finger-like shape to achieve effective contact over a multi-angle area [10]. Achieving congruence with the contact surface often necessitates a complex and precise sensing system design to ensure comprehensive coverage of the intended measuring area. Typically, these approaches have a clear and fixed size requirement of the sensing target. Another approach is to select a certain range of tactile data from the image and stitch it according to the motion strategy. In related studies, the method of data consolidation relies on the aggregation of small, centrally located, motion-captured image segments presumed to be at a uniform depth [11]. This method demands precise temporal synchronization and fails to harness tactile information across other image areas efficiently. Although curved structures provide structural feasibility for continuous detection scenarios, including objects larger than the sensor size or continuous non-stop production lines, this curvature challenges the consistency of captured contact depth, and the camera's focal plane, typically aligned with the surface, can result in out-of-focus imaging. This complicates the consistency and usability of the data. It is of concern that the elastomer deformation information and contact structure information contained in the acquired tactile data should be

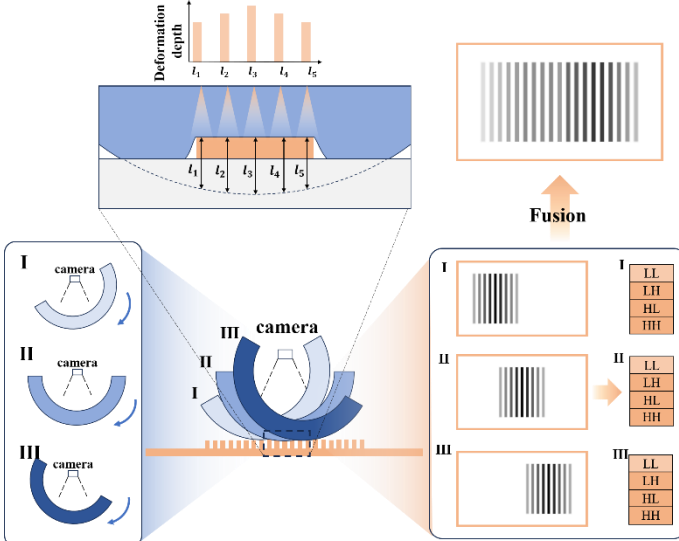


Fig. 1. The principle of the proposed cycle fusion strategy. Curved surface structure permits continuous contact and acquisition of the object while the sensor is rolling. During a single acquisition, due to the characteristics of the curved surface contact structure, the deformations generated at different positions of the sensor are inconsistent. The effect of fusion and the main processes of the fusion strategy are demonstrated in a 3D distribution of simulated data.

identifiable and separable in a defined sensing system. Meanwhile, on a series of tactile images obtained during the acquisition process, the actual tactile information can be fused by analyzing and filtering the features between the images.

To synthesize elastomer deformation information and overcome the interference of inconsistent contact depths, we propose a cyclic fusion strategy for vision-based tactile sensing. In the fusion strategy, the stitching of actual contact data is realized by fusing tactile information from multiple images. Considering these images encapsulate diverse contact states at varying depths and are distributed across an image sequence, the strategy extracts the overall features and edge features of the object's contact in the frequency domain. Further, different features in the tactile image are taken for different fusion computations around the contact depth distribution feature of the surface structure to retain the effective part of it. The tactile images obtained by utilizing this strategy are over 40% more informative while preserving structural similarity compared to the original single image obtained by the same sensing system and the stitched image using selected regions. The ability of the fusion strategy on the scale of a hundred micrometers is verified using tactile information at the pixel level in tactile images. In the discussion of tactile information contained in the pixel distribution of tactile images, the feature recognition capability of the tiny tactile information on the image is verified in conjunction with neural networks. It achieved a target detection mAP value of 90.90% and a classification accuracy of 99.83%, proving that the images contain information capable of distinguishing the tiny feature

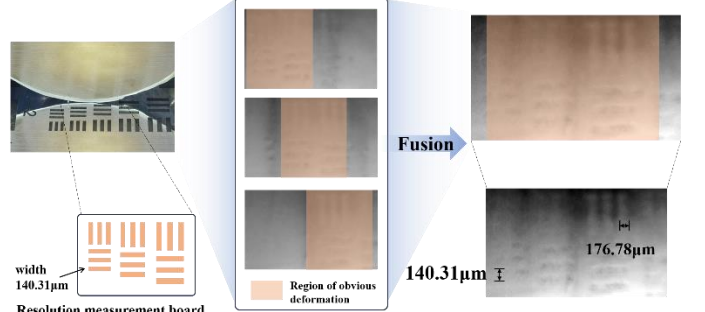


Fig. 2. Data acquisition and fusion performed at the resolution measurement board.

differences of the contacting objects. With the proposed cyclic fusion strategy, it can be achieved to remove the data interference from the contact structure for the successive acquisition of tactile information and thereby fusing and highlighting the information representing the actual morphology of the object on a tactile image, which facilitates the restoration of tactile sensations.

II. PRINCIPLES AND REASONS FOR FUSION

A. Principles of cycle fusion strategy

Despite advanced processing techniques like multi-scale analysis [12], and wavefront optimization [13], each with unique advantages for image fusion, the fusion of contact surface data encompassing information transmission mechanisms and contact dynamics, remains underexplored. By filtering the actual elastomeric shape variables from continuously collected tactile data, combined with the high resolution of tactile images, the integration of object contact samples in pixel fusion can be achieved and theoretically generalized to similar surface contacts. Fig.1 illustrates the principle of proposed cycle fusion strategy. Tactile information about different locations of the object is captured by scrolling, they are contact captures of different locations of the object and also varying contact depths for tactile information present in the same image. The sensing unit in the camera transforms the morphometric variables on tiny areas and presents them as pixel values. The strategy summarizes the information that reflects the actual shape of the contact location in the image and presents it in a single image. This approach was applied in minor deformations, capturing the texture of a 0.1 mm bump in a resolution measurement board as a tactile image, illustrated in Fig.2.

B. Contribution of curved surface structures to tactile images

In an acquisition sequence, distinct deformations are reflected in different regions of the image. The fusion strategy facilitates the integration of deformation data transmitted through the elastomer, allowing precise merging at the micrometer scale. To practically conduct the experimental discussion, the cylindrical vision-based tactile sensing system specifying the elastic contact structure of the curved surface as the region covering the outer surface of the cylinder was fabricated. This structure has been reported to be utilized in

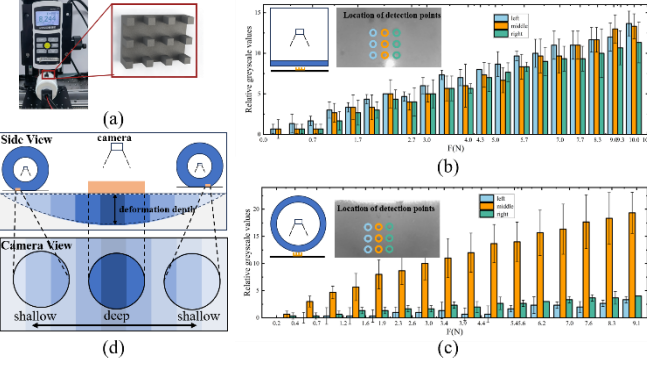


Fig. 3. (a) The scenario of the test. (b)(c) The schematic diagrams of the testing of the planar and curve structures, the location of the sampling point, and the relationship between the magnitude of the normal force and the amount of change in pixel value when pressed at different locations. (d) The different contact depth data was collected during contact with the object.

detection tasks [14][15]. The PDMS [16] assumed the functions of light transmission and flexibility..

The cylindrical vision-based tactile sensor structure is distinct in its image content compared to planar sensors which is made notable in the comparison. The vision-based tactile sensor for contrasting planar contact areas was prepared using the same materials and processes. The sensor was placed on the test platform employing a force gauge and displacement stage for testing, shown in Fig.3(a). A 3D-printed matrix probe, composed of 4x3 rectangular structures (1 mm x 1 mm x 2 mm) with 2 mm spacing, was mounted on the force gauge to evaluate deformation characteristics. Deformational characteristics were indicated by measuring the difference in gray values between images taken at sampling locations and images captured when no force was applied. Due to the presence of three points that did not produce a significant deformation response in the curved surface structure, three equidistant sampling points were chosen on each side of the contact area. In Fig.3(b), we observe that the planar structure exhibits uniform deformation across its regions. In contrast, Fig.3(c) shows that the change in gray value in the middle of the cylindrical structure is significantly higher than the sides. This shows that the cylindrical structure causes the center region to have a greater contact depth for the same force, resulting in greater deformation. The regions on the sides show a gradual response as the force increases. When the sensor contacts an object, some region of the contact layer detects varying levels of deformation due to the hard material. As the sensor rolls, the contact process progresses from edge to center and then back to the edge, effectively capturing contact information at various depths. It starts from a shallow depth, progresses to a deeper level, and then returns to a shallower depth within a localized area. Simultaneously, though the contact surfaces of the probes make the

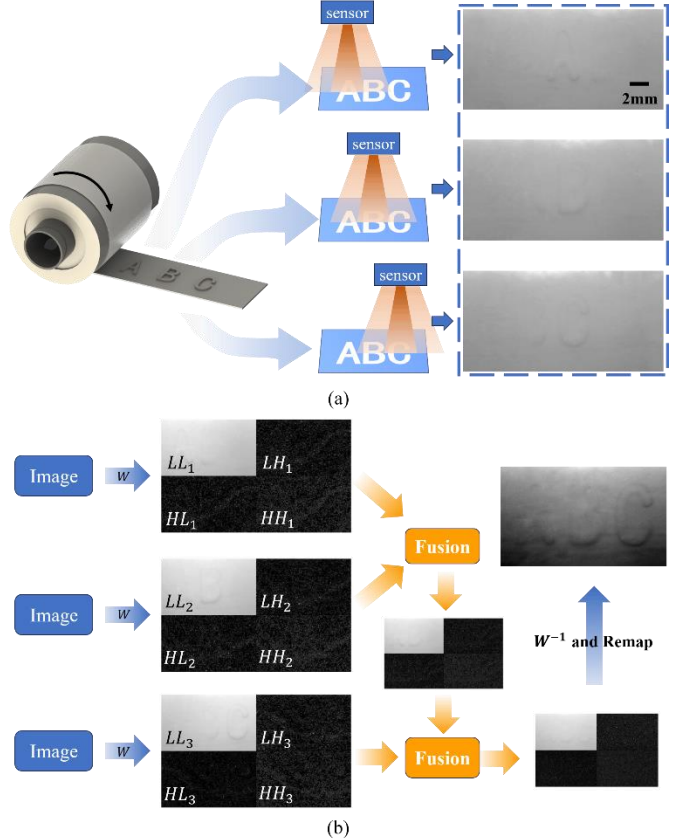


Fig. 4. (a) Demonstration of image acquisition and original image undergoing fusion. Scale relationships are labeled in the tactile images on top, and apply to all tactile images in this figure. (b) Demonstration of the cyclic fusion process.

deformations of each position different, their positions in the image correspond with the actual positions, ensuring a faithful representation of relative spatial relationships.

In a vision-based tactile sensor, the images hold measuring information captured by the camera, reflecting changes in the flexible contact layer via optical signals. The encoding of contact deformation by optical information can be analyzed using Lambert's cosine law [17]. From the whole image, the deformation induced by an object in contact with the sensor is not uniform for each region of the flexible contact layer due to the cylindrical structure. This results in the acquired tactile images containing deformation data from different contact depths. As the sensor rolls, different sensor regions come into contact with the object, as shown in Fig.3(d). This means that the appearance of the object is contained at various locations in the acquired images within a region. Each tactile image records contact data at various depths within a region. And there is a mixture of valuable data and disturbing data. Therefore, the selection and integration of contact data in the image sequence that can construct the actual appearance of the object is a critical part of surface contact data processing.

III. FUSION USING IMAGE SEQUENCES

A. Processes and methods of fusion

Analyzing contact depth disparities attributed to surface structure nuances underscores the imperative for a streamlined and potent data processing approach. From the analysis, it can be obtained that there is potentially complementary information, despite the displacement of the objects and the non-corresponding presentation of the contact data in each image. Analyzing contact depth disparities attributed to surface structure nuances underscores the imperative for a streamlined and potent data processing approach. When this information is effectively integrated, it will provide a comprehensive and accurate description of the contact state. Therefore, we propose a cyclic fusion strategy. This is achieved through cyclic extraction and amalgamation of preceding and succeeding images in the sequence.

Since the target has a certain projected area, the image sequence containing the target exhibits distributed contact data from these deepest positions after rolling acquisition by the sensor. The task is to extract and fuse the contact data containing the target object. In an image sequence, the whole shape of the object and the edge information are present at different frequencies, which can be used to identify the object's actual shape, so it is important to separate them from the background and the noise. Confronted with this necessity, Daubechies wavelet transform [18] becomes an important tool. This transform can decompose an image at multiple resolutions so that the important frequency components can be separated. Fig.4(a) illustrates the acquisition process and the original image of an alphabet image sequence. As the sensor rolls during acquisition, the object shifts position within the image. The template-matching algorithm [19] was used to correct the image alignment error caused by the sensor shifts, to make the spatial distribution of the object features in the fused images as consistent as possible. The process of fusion is shown in Fig.4(b). Wavelet transform is applied to the image to obtain:

$$W(I) = \{LL, LH, HL, HH\} \quad (1)$$

where $W(I)$ refers to performing wavelet transform on image I . LL is the low-frequency component, which is used to capture the basic structure and global features of the object. LH , HL and HH are the three high-frequency components. They are computed in the horizontal, vertical, and diagonal directions, respectively, and carry subtle features such as edges and details. Applying wavelet transform allows us to independently distinguish and process different frequency components of an image. Meanwhile, the wavelet transform is highly sensitive to sharp regions in the image, usually the edges of objects and texture mutations, which means that the features in these regions will be extracted efficiently, and thus more easily recognized and preserved in the subsequent fusion process, ultimately retaining as much visually important information as possible.

Various fusion strategies are used for the subbands to cope

with different features. The low-frequency subbands are fused equally, while the high-frequency subbands are assigned different weights for fusion after a significance analysis. With different fusion strategies, on the one hand, averaging the low-frequency subbands ensures the consistency of the fused images in terms of visual continuity and scene structure based on random noise reduction. On the other hand, the clarity of detail in the image is strengthened by performing saliency analysis and weighted fusion on the high-frequency subbands. The saliency analysis ensures that the fusion process pays more attention to the regions that are more significant for the comprehension of the scene, which presents the more informative and visually essential parts of the image. The fusion process is represented as:

$$F_{LL} = \frac{LL_1 + LL_2}{2} \quad (2)$$

$$Sal(I) = \left(\frac{|\frac{\partial^2 I}{\partial x^2} + \frac{\partial^2 I}{\partial y^2}|}{\max(|\frac{\partial^2 I}{\partial x^2} + \frac{\partial^2 I}{\partial y^2}|)} \right) \times 255 \quad (3)$$

$$S = \exp \left(\frac{Sal(I)}{255} \right) - 1 \quad (4)$$

$$W_1 = \frac{S_1}{S_1 + S_2}, \quad W_2 = 1 - W_1 \quad (5)$$

$$F_{HS} = HS_1 \cdot W_1 + HS_2 \cdot W_2, \quad HS = \{LH, HL, HH\} \quad (6)$$

where F_{LL} denotes the fused low-frequency subband and LL_1, LL_2 denotes the low-frequency subband of the two images involved in the fusion. $Sal(I)$ represents the saliency map of an image, represented through second-order derivation of the image and transformed to a range of grey values. S is the adjusted saliency map, which aims to optimize the distribution of salient components. Further, the weights W_1 and W_2 in the fusion can be obtained from the saliency maps S_1 and S_2 of the two images and F_{HS} represents the fused high-frequency subbands with three specific results LH , HL and HH . The fused subbands are converted back to the spatial domain by wavelet inverse transformation to get the fused image:

$$I_f = W^{-1}(F_{LL}, F_{LH}, F_{HL}, F_{HH}) \quad (7)$$

where W^{-1} denotes the wavelet inverse transform. I_f is the fused data remapped to grayscale. Afterward, the fused data is fused with the next image in the sequence as a new image by cyclic fusion strategy, and the process is repeated until completion. The cyclic fusion strategy is employed to fully utilize the effective information provided by each frame in the sequence to build up a complete and detail-rich image gradually. By performing the same transformation and fusion process of the fused image with the next image in the sequence, the detailed information on the critical areas can be gradually enhanced in each step and ensure that the fusion result maintains visual and informational coherence throughout the sequence. The fused image takes the actual measuring information (clear alphabets seen in image), which initially existed in separate images, and fuses them on a single image. This shows that our method realizes the splicing of

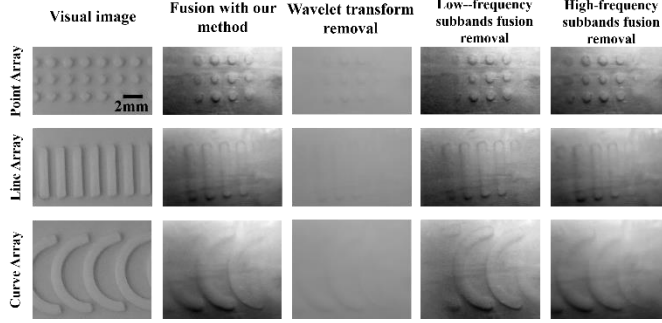


Fig. 5. Results of the ablation experiment. Shows visual images captured by the camera, fusion images using our method, and the fusion images obtained from the three sets of ablation experiments from left to right for the three pattern samples. A 2 mm width label is marked out in the tactile image on top, which applies to all images in this figure.

TABLE I
RESULTS OF ABLATION EXPERIMENTS

motifs	metrics	Fusion with our method	Wavelet Transform Removal	Low-frequency Subbands Fusion Removal	High-frequency Subbands Fusion Removal
point	IE	7.5814	4.91068	7.6178	7.5047
	MS-SSIM	0.2231	0.6046	0.1930	0.2370
line	IE	7.5077	5.2018	7.4953	7.4977
	MS-SSIM	0.5470	0.8207	0.4998	0.5540
curve	IE	7.6736	5.4270	7.5711	7.6927
	MS-SSIM	0.3290	0.5984	0.3224	0.3310

effective information in the contact process. The acquisition of sequences containing different numbers of images can be continuous with uniform pressure application. This means that the number of images to be fused is adjustable and can be adapted to scenes with more complex textures.

B. Effectiveness evaluation of fusion

The idea of ablation experiments [20] was adopted for validation to evaluate the effectiveness of the proposed image fusion strategy. By systematically removing the key steps in the fusion process, it aims to reveal the contribution of each part of the fusion strategy to the final fusion effect. Three main operations were performed ablation: the application of wavelet transform, the averaging fusion of the low-frequency subbands, and the fusion of the high-frequency subbands with weights assigned based on significance analysis. Specifically, the value of the wavelet transform was first compared by performing a direct averaging calculation of the pixels instead of applying the wavelet transform. Second, the contribution of the low-frequency part of the fusion is verified by selecting the low-frequency subbands of one image instead of the mean fusion of the low-frequency subbands of all images of the image sequence. Lastly, the weights of the adaptive high-frequency information obtained utilizing significance analysis are ignored and substituted for the information selected as the highest value. This idea typically means that the most salient portion of each section represents the sensitive information that receives the most attention.

For comparison, standardized samples were designed and produced to validate the proposed strategy. An image matrix elevated 1 mm from the plane was created for the experiment,

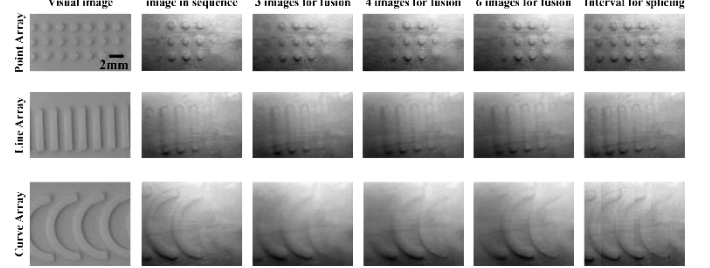


Fig. 6. Test results in the graphic matrices. Shows the original image, different numbers of fusion results, and the splicing performed using the sensor motion-based time sampling stitching method. A 2 mm width label is marked out in the tactile image on top, which applies to all images in this figure.

TABLE II
RESULTS OF COMPARISON OF METHODS AND QUANTITATIVE STRATEGIES

motifs	metrics	single image	fusion 3 images	fusion 4 images	fusion 6 images	time-splicing
point	IE	4.9255	7.5111	7.5814	7.6193	4.8792
	MS-SSIM	0.4631	0.4589	0.4508	0.4441	0.4663
line	IE	5.2213	7.5068	7.5077	7.5293	5.2224
	MS-SSIM	0.6307	0.6397	0.6418	0.6375	0.6183
curve	IE	5.5061	7.6912	7.6736	7.6496	5.4369
	MS-SSIM	0.5049	0.4948	0.4964	0.5009	0.4980

with points, lines, and curves as pattern units. Two metrics were used to evaluate the performance of the proposed strategy: Information Entropy (IE) [21] and Multi-Scale Structural Similarity Index (MS-SSIM) [22]. IE measures the information richness of an image, which is the uncertainty in the distribution of image pixels, and a high value of information entropy indicates that the image contains more information. The purpose of choosing IE as a metric is to directly assess the amount of information in the fused image and determine whether the fusion operation effectively enhances the image content. MS-SSIM is used to quantify the visual similarity between the fused image and a selected reference image to assess the ability of the fused image to maintain the original visual information and structure. An optical image of a standardized sample taken directly through the camera as the reference image and scaled to a consistent scale. MS-SSIM was chosen as the evaluation metric because it reflects the maintenance and enhancement of image quality during the fusion process. Thus, the combination of MS-SSIM and IE provides a comprehensive framework for assessing both the visual accuracy of the fused images and measuring the increase in their information content, which is essential for validating the effectiveness of image fusion methods. The fusion process uses four images obtained from an acquisition. The results are shown in Fig. 5 and Table. I.

The results show that after removing one step, the majority of the IE values show a decrease. In particular, the fusion without wavelet transform fails to present the primary information of the images, both in terms of metrics and visual effects. In the case of MS-SSIM, the fusion without wavelet transform achieves high results because it averages the pixel distribution area in the image, which is similar to the effect in the visual image. The other results are relatively similar. The

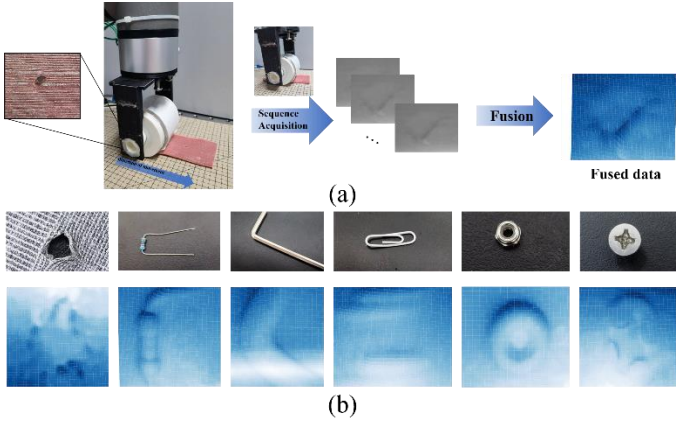


Fig. 7. (a) Sensors are used in combination with robotic arms for the process and results of object contact acquisition. (b) Application demonstrations on daily objects.

strategy's overall quantitative metrics and visual results are more balanced than the fusion strategy which removes one step. Meanwhile, the fusion strategy is relatively more robust for pattern features with different complexity, such as points and curves in the experiment whose feature complexity differs. In addition, the strategy also performs more consistently in removing noise and highlighting features on visual images. For example, there is blurring of the edges of the pattern in the image with the removal of the high-frequency subbands fusion strategy.

The effectiveness of the strategy was evaluated through comparison experiments. A sequence of images was captured using the sensor and a different number of images were for fusion. For contrast, single images from the sequence and images using the sensor motion-based time sampling stitching method were also tested. Due to the different distribution of information in different fusion strategies, the images undergoing evaluation are normalized for gray values to unify the mapping relationships, as shown in Fig. 6 and Table II. All the elements in the single images from the sequence and images using the sensor motion-based time sampling stitching method are directly derived from the acquired raw data and thus have a natural advantage in terms of similarity. Our proposed cyclic fusion strategies significantly improve the IE values by over 40% while maintaining the same MS-SSIM values as these images. This result demonstrates that image features can be effectively extracted and enhanced through our approach without compromising the integrity and reliability of the original information. Specifically, the wavelet transform allows us to process different frequency components independently and identify and assign higher weights to critical regions for tactile perception. This approach is expected to enhance the tactile character and informativeness of the image, and the enhancement of the IE values is proof of this expectation. Meanwhile, the maintenance of the MS-SSIM values indicates that the fused image is comparable to the original image in terms of visual quality. Our fusion method enhances the tactile information without losing visual quality. The experiments have also shown that the number of

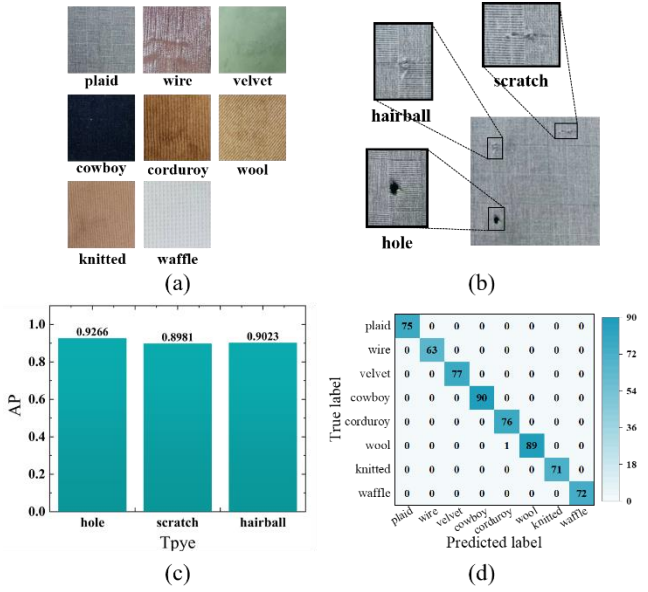


Fig. 8. (a)(b) Samples used to produce the dataset, include eight fabrics and three defects. (c) AP values of defect detection targets. (d) Confusion matrix for the category classification task.

images involved in fusion has an inconsistent correlation with the results in different scenes. But basically, it does not change the level of the metrics. Therefore, the number of samples required for performing fusion depends on the scene in the actual task.

IV. STRATEGY APPLICATION AND EXPANSION DISCUSSION

Experiments show the process and results of performing contact information acquisition on daily objects. As shown in Fig.7(a), the sensor is connected to a robotic arm that can make contact with the object to be acquired, and the acquired image sequence is fused by our method. The figure shows the process of detecting a defective area of a piece of fabric, the captured raw image, and the result of remapping based on the distribution of the fused data. Fig.7(b) shows the effect on everyday objects such as screws, paper clips, and other objects. The image after fusion is performed can present a larger area of the object and more details. However, it is worth noting that the sensor's capability to obtain morphological information effectively is limited for areas with depths beyond the reach of the sensor's flexible contact layer. For example, the texture deeper in the middle region of the screw head cannot be captured. The requirement for different depths of detection can be realized by modifying the size of the sensor's contact layer or by altering the flexible material.

In previous sections, the cyclic fusion strategy is used in the image sequence. Although this work focuses on enhancing image features through fusion, it can be found that single images in an image sequence have independent value and application potential under specific conditions. For example, in target detection or category classification applications, even though single images are deficient in the continuity and

capacity of target features due to the limitations of the contact surface structure, they can still record features reflecting some specific attributes of the object. It is considered that this feature has the opportunity to have the potential for the combined use of single and fused images. We discuss it through a test using neural networks[23][24].

In the discussion, a CenterNet neural network [25] using ResNet [26] as the backbone of the feature extraction network was developed. Meanwhile, for the output structure of the network, an output branch was added for overall category classification to enable the network to take on both target detection [27] and category classification [28] tasks. We performed experiments on fabric samples. As shown in Fig.8(a) and Fig.8(b), eight fabric samples were used to test the classification capability, and three different defect types were used to test the target detection capability. Vision-based tactile sensing system was used to touch and acquire images of the fabrics and label them with information. The weight with the lowest loss value of the validation set in 150 epochs is used for performance evaluation. Regarding defect detection performance, the experiment yielded a mAP value of 90.90% when the Score Threshold was set to 0.5. Fig.8(c) shows the AP. For the classification task, the confusion matrix in Fig.8(d) highlights a remarkable accuracy of 99.83%. The algorithm overcomes the difficulty of inhomogeneous feature information in images and performs strongly in extracting texture features. Real-time detection is critical in practical applications, and the curved surface sensor's design lends itself to dynamic and continuous detection. By continuously detecting 100 images and recording the time taken, an FPS of 47.214 is obtained. Experiments verified the outstanding discriminative ability of a single image in detecting defective targets and identifying relevant object classes, which emphasizes the reliability of image sequences in single-image applications.

V. CONCLUSION

In this work, we propose a cyclic fusion strategy to fusion and present actual elastomer deformations in curved surface contact. For the situation that surface contact data are at different depths due to the curved surface contact structure, we use cyclic fusion to extract and integrate the data that characterize the object features by combining the characteristics of the contact depths and the changing properties of the object features in the image. A cylindrical vision-based tactile sensing system with typical curved contact characteristics is fabricated for testing and discussion. The cyclic fusion is performed by cyclically performing wavelet transform followed by averaging fusion and fusion based on significance analysis for the low-frequency and high-frequency components. The tactile images fused with our proposed strategy have over 40% more information and similar structural similarity as compared to the single images captured by the sensing system and the images obtained using the sampling stitching method. Further, in combination with neural networks, we discuss the tactile information present in

the pixel distribution in a single tactile image. The results show high accuracy and application potential, which specifically include a classification accuracy of 99.83% and a target detection mAP of 90.90%. Our approach both overcomes the lack of non-uniform depth present in curved contact structures and extends the study with potential applications utilizing structural features. Combining the immediacy of single images with the comprehensiveness of fused images, we foresee a new multimodal sensing paradigm with feasibility. The sensor needs to scan the object only once to obtain an exhaustive data set. This approach not only improves detection efficiency and reduces repetitive work but also enhances the recognition of object features by utilizing a single image's high resolution and detail information while maintaining the continuity of haptic perception. In addition, combining single images and fused images can bring higher flexibility and adaptability to the tactile sensing system and achieve optimal allocation of resources. Future improvements in our work include integrating the sensor hardware and the algorithm's robustness.

REFERENCES

- [1] H. Meng, L. Zhou, X. Qian and G. Bao, "Design and Application of Flexible Resistive Tactile Sensor Based on Short-Circuit Effect," *IEEE Transactions on Instrumentation and Measurement*, vol. 72, pp. 1-8, 2023, no. 9501008, doi: 10.1109/TIM.2022.3225063.
- [2] D. Zhong, et al, "High-speed and large-scale intrinsically stretchable integrated circuits," *Nature*, vol. 627, pp.313-320, 2024, doi: 10.1038/s41586-024-07096-7.
- [3] B. W. An, S. Heo, S. Ji, F. Bien, and J. Park, "Transparent and flexible fingerprint sensor array with multiplexed detection of tactile pressure and skin temperature," *Nature Communications*, vol. 9, no. 2458, Jul. 2018, doi: 10.1038/s41467-018-04906-1.
- [4] Z. Zou, et al. "Monitoring Soft Shape Surface Deformation via Optical Images for the Distinction of Contact State," *Advanced Intelligent Systems*, vol. 6, no. 3, 2024, doi: 10.1002/aisy.202300535.
- [5] M. Alshawabkeh et al., "Highly Stretchable Additively Manufactured Capacitive Proximity and Tactile Sensors for Soft Robotic Systems," *IEEE Transactions on Instrumentation and Measurement*, vol. 72, pp. 1-10, 2023, no. 7502210, doi: 10.1109/TIM.2023.3250232.
- [6] G. Dingley, M. Cox and M. Soleimani, "EM-Skin: An Artificial Robotic Skin Using Magnetic Inductance Tomography," *IEEE Transactions on Instrumentation and Measurement*, vol. 72, pp. 1-9, 2023, no. 4503309, doi: 10.1109/TIM.2023.3268481.
- [7] G. H. Yang, W. Lee, and S. Kang, "Development of vibrotactile pedestal with multiple actuators and application of haptic illusions for information delivery," *IEEE Transactions on Industrial Informatics*, vol. 15, no. 1, pp. 591-598, Jan. 2019, doi: 10.1109/TII.2018.2850849.
- [8] M. Li, L. Zhang, T. Li and Y. Jiang, "Continuous Marker Patterns for Representing Contact Information in Vision-Based Tactile Sensor: Principle, Algorithm, and Verification," *IEEE Transactions on Instrumentation and Measurement*, vol. 71, pp. 1-12, 2022, no. 5018212, doi: 10.1109/TIM.2022.3196730.
- [9] W. Xu, et al, "A Vision-Based Tactile Sensing System for Multimodal Contact Information Perception via Neural Network," 2023, arXiv:2310.01986.
- [10] B. Ward-Cherrier et al, "The TacTip Family: Soft Optical Tactile Sensors with 3D-Printed Biomimetic Morphologies," *Soft Robotics*, vol. 5, no.2, pp. 216-227, Apr. 2018, doi: 10.1089/soro.2017.0052.
- [11] K. Shimonomura, T. Chang, and T. Murata, "Detection of Foreign Bodies in Soft Foods Employing Tactile Image Sensor," *Front Robot AI*, vol. 8, Dec. 2021, doi: 10.3389/frobt.2021.774080.
- [12] C. Ji, W. Zhou, J. Lei and L. Ye, "Infrared and Visible Image Fusion via Multiscale Receptive Field Amplification Fusion Network," *IEEE Signal*

Processing Letters, vol. 30, pp. 493-497, 2023, doi: 10.1109/LSP.2023.3270759.

[13] L. Liu, W. Li, M. Gong, L. Zhong, H. Gu and S. Liu, "Resolution-Enhanced Lensless Ptychographic Microscope Based on Maximum-Likelihood High-Dynamic-Range Image Fusion," IEEE Transactions on Instrumentation and Measurement, vol. 73, pp. 1-11, 2024, Art no. 4502711, doi: 10.1109/TIM.2024.3363788.

[14] G. Cao, J. Jiang, C. Lu, D. F. Gomes, and S. Luo, "TouchRoller: A Rolling Optical Tactile Sensor for Rapid Assessment of Textures for Large Surface Areas," Sensors, vol. 23, no. 5, pp. 2661, Feb. 2023, doi: 10.3390/s23052661.

[15] B. Fang, X. Long, F. Sun, H. Liu, S. Zhang, and C. Fang, "Tactile-Based Fabric Defect Detection Using Convolutional Neural Network With Attention Mechanism," IEEE Transactions on Instrumentation and Measurement, vol. 71, pp. 1-9, May. 2022, doi: 10.1109/TIM.2022.3165254.

[16] S. B. Campbell, Q. Wu, J. Yazbeck, C. Liu, S. Okhovatian, and M. Radisic, "Beyond Polydimethylsiloxane: Alternative Materials for Fabrication of Organ-on-a-Chip Devices and Microphysiological Systems," ACS Biomaterials Science & Engineering, vol. 7, no. 7, pp. 2880-2899, Aug. 2020, doi: 10.1021/acsbiomaterials.0c00640.

[17] J. Folkesson, H. Chang, and N. Bore, "Lambert's Cosine Law and Sidescan Sonar Modeling," 2020 IEEE/OES Autonomous Underwater Vehicles Symposium (AUV), St. Johns, NL, Canada, 2020, pp. 1-6, doi: 10.1109/AUV50043.2020.9267946.

[18] S. A. Cortez, L. Bokati, A. Velasco and V. Kreinovich, "Why Daubechies Wavelets Are so Successful," Journal of Intelligent & Fuzzy Systems, vol. 43, no. 6, pp. 6933-6938, Nov. 2022, doi: 10.3233/JIFS-212021.

[19] Y. Ye, L. Bruzzone, J. Shan, F. Bovolo and Q. Zhu, "Fast and Robust Matching for Multimodal Remote Sensing Image Registration," IEEE Transactions on Geoscience and Remote Sensing, vol. 57, no. 11, pp. 9059-9070, Nov. 2019, doi: 10.1109/TGRS.2019.2924684.

[20] J. Li, B. Yang, L. Bai, H. Dou, C. Li and L. Ma, "TFIV: Multigrained Token Fusion for Infrared and Visible Image via Transformer," IEEE Transactions on Instrumentation and Measurement, vol. 72, pp. 1-14, 2023, no. 2526414, doi: 10.1109/TIM.2023.3312755.

[21] Z. Wang, D. He, Z. Wang and Q. Li, "Timeliness and Stability-Based Operation Optimization for Copper Flotation Industrial Process," IEEE Transactions on Instrumentation and Measurement, vol. 72, pp. 1-12, 2023, no. 3500912, doi: 10.1109/TIM.2022.3225924.

[22] Y. Yang, Y. Zhang, S. Huang, Y. Zuo and J. Sun, "Infrared and Visible Image Fusion Using Visual Saliency Sparse Representation and Detail Injection Model," IEEE Transactions on Instrumentation and Measurement, vol. 70, pp. 1-15, 2021, no. 5001715, doi: 10.1109/TIM.2020.3011766.

[23] S. Zhang et al., "A Compact Visuo-tactile Robotic Skin for Micron-level Tactile Perception," IEEE Sensors Journal, doi: 10.1109/JSEN.2024.3376574.

[24] H. Wang, J. Wang, Y. Zhao, Q. Liu, M. Liu and W. Shen, "Few-Shot Learning for Fault Diagnosis With a Dual Graph Neural Network," IEEE Transactions on Industrial Informatics, vol. 19, no. 2, pp. 1559-1568, Feb. 2023, doi: 10.1109/TII.2022.3205373.

[25] X. Zhou, D. Wang, and P. Krähenbühl, "Objects as Points," Apr. 2019. [Online]. Available: arXiv: Computer Vision and Pattern Recognition, doi: 10.48550/arXiv.1904.07850.

[26] K. He, X. Zhang, S. Ren, and J. Sun, "Deep Residual Learning for Image Recognition," 2016 IEEE Conference on Computer Vision and Pattern Recognition (CVPR), Las Vegas, NV, USA, 2016, pp. 770-778, doi: 10.1109/CVPR.2016.90.

[27] J. Li et al., "Automatic Detection and Classification System of Domestic Waste via Multimodel Cascaded Convolutional Neural Network," IEEE Transactions on Industrial Informatics, vol. 18, no. 1, pp. 163-173, Jan. 2022, doi: 10.1109/TII.2021.3085669.

[28] C. Jiang, et al., "Neuromorphic antennal sensory system," Nature Communications, vol. 15, no. 2109, 2024, doi: 10.1038/s41467-024-46393-7.



Zilan Li. He has received the B.S. degree in South China Normal University, Guangzhou, China, in 2023. He is currently occupied in his M.S. degree in South China Normal University, Guangzhou, China. His currently interests include Optoelectronic intelligent sensing and deep learning.



Zhibin Zou. He has received the B.S. degree in Huaqiao University, Xiamen, China. He is currently occupied in his M.S. degree in South China Normal University, Guangzhou, China. His currently interests include optoelectronic technology and intelligent sensing.



Weiliang Xu received B.S. degree in South China Normal University, Guangzhou, China, in 2022. He is currently occupied in his Ph.D. degree in South China Normal University, Guangzhou, China. His current interests include Human-Computer Interaction and optoelectronic intelligent sensing design.



Yuanzhi Zhou. He was received B.S. degree in School of Physics, Hefei University of Technology, Hefei, China. He is currently occupied in his Ph.D. degree in South China Normal University, Guangzhou, China. His current interests include Human-Computer Interaction and intelligent system design.



Guoyuan Zhou received the bachelor's degree in Optical Information Science Engineering from Nanjing Tech University. He is currently occupied Ph.D. in South China Normal University. His current interests include vision-based tactile sensors.



Muxing Huang. He is currently occupied in his B.S. degree in South China Normal University, Guangzhou, China. His currently interests include Optoelectronic intelligent sensing and intelligent control system.



Xuan Huang. She received her B.S. degree from Yanshan University in Qinhuangdao, Hebei, China in 2021. She is currently pursuing a M.S. degree in the South China Normal University in Guangzhou, Guangdong Province, China. Her current interests include flexible ionic electronics and intelligent sensing design.



Xinming Li received his B.Sc. and Ph.D. degrees from Tsinghua University in 2007 and 2013, respectively. After that, he was an Assistant Professor at the National Center for Nanoscience and Technology, China, postdoctoral research fellow at The Chinese University of Hong Kong, research fellow at The Hong Kong Polytechnic University, and JSPS postdoctoral Fellow at the National Institute for Materials Science, Japan. He is currently a Professor with the School of Information and Optoelectronic Science and Engineering, at South China Normal University, China. He has co-authored more than 90 journal publications. His research interests include wearable devices, optoelectronic technology, vision-based tactile sensors, intelligent sensing systems, and haptics technology. He served as editor for Sensors, and Frontiers in Physics.